Stationary nanoliter droplet array with a substrate of choice for single adherent/nonadherent cell incubation and analysis

Jonathan Shemesh[a,b], Tom Ben Arye[a,b], Jonathan Avesar[a], Joo H. Kang[c,d], Amir Fine[a], Michael Super[c], Amit Meller[a,b], Donald E. Ingber[c,d,e], and Shulamit Levenberg[a,b,1]

[a]Department of Biomedical Engineering and [b]Russell Berrie Nanotechnology Institute, Technion—Israel Institute of Technology, Haifa 32000, Israel; [c]Wyss Institute for Biologically Inspired Engineering, Harvard University, Boston, MA 02115; [d]Harvard School of Engineering and Applied Sciences, Cambridge, MA 02139; and [e]Vascular Biology Program, Boston Children's Hospital and Harvard Medical School, Boston, MA 02115

Edited by Robert Langer, Massachusetts Institute of Technology, Cambridge, MA, and approved June 24, 2014 (received for review March 10, 2014)

Microfluidic water-in-oil droplets that serve as separate, chemically isolated compartments can be applied for single-cell analysis; however, to investigate encapsulated cells effectively over prolonged time periods, an array of droplets must remain stationary on a versatile substrate for optimal cell compatibility. We present here a platform of unique geometry and substrate versatility that generates a stationary nanodroplet array by using wells branching off a main microfluidic channel. These droplets are confined by multiple sides of a nanowell and are in direct contact with a biocompatible substrate of choice. The device is operated by a unique and reversed loading procedure that eliminates the need for fine pressure control or external tubing. Fluorocarbon oil isolates the droplets and provides soluble oxygen for the cells. By using this approach, the metabolic activity of single adherent cells was monitored continuously over time, and the concentration of viable pathogens in blood-derived samples was determined directly by measuring the number of colony-formed droplets. The method is simple to operate, requires a few microliters of reagent volume, is portable, is reusable, and allows for cell retrieval. This technology may be particularly useful for multiplexed assays for which prolonged and simultaneous visual inspection of many isolated single adherent or nonadherent cells is required.

single cell | nanoliter array | diagnostics

Common single-cell analysis methods, such as flow cytometry and mass cytometry (1), offer high throughput and accurate single-cell marker quantification, yet they lack the ability to monitor large numbers of single cells continuously and simultaneously in performance-based assays (2, 3). Conventional microscopy may be used for these assays; however, in the case of single cells, they cannot analyze extracellular events, such as secretion. To achieve this, cells must be isolated in compartments that can sustain cell viability and growth while permitting conventional optical analysis over many hours to days. Droplet-based microfluidics, which enables single-cell encapsulation in nano- and subnanoliter droplets by surrounding microscopic aqueous medium with an immiscible carrier fluid (4–8), recently gained interest with the appearance of digital PCR (9–11). Much of the work thus far has been directed toward improving droplet manipulation capabilities (12–16). With these methods, droplets are mobile, and thus cytometry is performed under flow conditions (17), making continuous monitoring of single cells difficult. Continuous monitoring may be achieved by using stationary indexed droplets, but many current droplet immobilization techniques are limited by pressure coupling between droplet generation and capture events, as well as the requirement to adjust droplet volume to nanowell size (6, 18, 19). The vast majority of methods used to generate water-in-oil droplets begin by priming a continuous oil phase in a microfluidic channel followed by an injection of a dispersed (aqueous) medium (20–22). Using these approaches, droplets can be trapped by surface energy minimization. However, the interfacial energy has one constant value dictated by the chemical properties of the oil and dispersed media, leaving only the parameter of nanowell geometry to achieve droplet immobilization and limiting these techniques to finely tuned loading pressures and the use of tubing. In addition, because the droplets in the above methods are fully sheathed by a carrier fluid, they are designed primarily for studies with suspended cells. There are methods that bypass the production and capturing under flow altogether by initially producing stationary plugs within the geometry of the device (2, 23–25). However, upon their adjustment to prolonged mammalian assays, they require multilayer fabrication, either involving high-pressure cell loading or not allowing for different substrates to be used (26, 27). Several single-cell platforms that encapsulate cells in stationary droplet arrays are available (5, 28–35); however, the ability to culture adherent cells for long periods remains difficult (36).

Here, we demonstrate a microfluidic method to generate stationary nanodroplet arrays (SNDAs) rapidly and easily on a surface of choice (e.g., tissue culture plates, coverslips). It uses a loading procedure operated in reverse order, in which the dispersed medium is injected first and sheared into droplets, whereas a continuous phase is injected only subsequently for droplet sheathing. The system generates indexed stationary droplets, each with variable chemical composition, and can support both adherent and nonadherent cell culture.

Significance

There is a substantial need for single-cell platforms in which each cell is chemically isolated in its own microenvironment and a lack of such platforms that support adherent cells. We present here a method that generates stationary nanoliter droplet arrays on a substrate of choice and supports long-term incubation and interrogation of single cells. We demonstrate the encapsulation of single human dermal fibroblast cells and their substrate attachment, viability, and proliferation, and show they can be retrieved and interfaced to standard cell culturing techniques. We also demonstrate a single-cell metabolic assay and track it over selected groups of indexed traps. The device does not require external equipment or machinery, making it available for point-of-care applications.

Author contributions: J.S., T.B.A., J.A., J.H.K., M.S., A.M., D.E.I., and S.L. designed research; J.S., T.B.A., J.A., and J.H.K. performed research; A.F. contributed new reagents/analytic tools; J.S., T.B.A., J.A., J.H.K., M.S., D.E.I., and S.L. analyzed data; and J.S., T.B.A., J.A., J.H.K., A.M., D.E.I., and S.L. wrote the paper.

The authors declare no conflict of interest.

This article is a PNAS Direct Submission.

[1]To whom correspondence should be addressed. Email: shulamit@bm.technion.ac.il.

This article contains supporting information online at www.pnas.org/lookup/suppl/doi:10.1073/pnas.1404472111/-/DCSupplemental.

Downloaded at Palestinian Territory, occupied on December 14, 2021

www.manaraa.com

The platform is simple to fabricate and operate and provides the conditions and sustenance necessary for prolonged mammalian cell culture (3 d), making it suitable for single- or near-single–cell assays that require these long time scales. It uses a quick and low-pressure loading process, allows for proper oxygen exchange, and provides the flexibility of choosing the cell growth substrate, properties especially convenient for adherent cell culture.

Results

SNDA Operation and Performance Range. The main structural features of the SNDA include a sequence of nanowells branching off a main channel connected to secondary channels through narrow (6 ± 2-μm) restrictions within a polydimethylsiloxane (PDMS) microfluidic device (Fig. 1*A* and Fig. S1). To load the device (Fig. 1*B* and Movie S1), it first is attached to a flat surface of choice, such as glass or plastic, to form a hermetic yet reversible seal. An aqueous solution, which may contain cells, is injected by pressure into the main channel. During this step, air escapes the device through the secondary channels, yet the liquid is arrested by its limited liquid–gas meniscus curvature and surface tension dictated by the Laplace pressure at the restriction (Fig. 1 *b2*). Air pressure is then applied at the inlet to shear the dispersed media into separate droplets (Fig. 1 *b3*), which are stabilized by the trap's structure. In the last step, fluorocarbon oil is injected into the main and secondary channels. It flows with the aid of capillary forces and sheathes and chemically isolates the droplets (Fig. 1 *b4* and *b5* and Fig. S2). Air bubbles do not form, because the oil fully wets the elastomer surface. The fluorocarbon oil serves two purposes: it suppresses water evaporation and increases oxygen in the droplets because of its high oxygen solubility (37, 38).

During shearing, fluid segmentation is favored over liquid evacuation because of surface energy minimization. For example, it is known that sessile electro-wetting on dielectric water droplet fission is possible only when a droplet is squeezed between two surfaces (39), which is possible because of energy barrier reduction before and after droplet splitting. The energy change required to overcome such splitting is approximated by $\Delta E/E = (\sqrt{2}-1)/\left(1+\frac{\gamma_{SL}\cdot a}{\gamma_{LG}\cdot\delta}\right)$, where γ_{SL} and γ_{LG} are the surface–liquid and liquid–gas interfacial tensions, respectively; a is the droplet radius; and δ is the plate separation. In the case in which $\gamma_{SL}a \gg \gamma_{LG}\delta$, this reduces to $\Delta E/E \sim (\gamma_{LG}\cdot\delta)/(\gamma_{SL}\cdot a)$. Namely, for a given interfacial tension, to induce droplet fission, the liquid–surface contact area should be maximized in favor of the liquid–gas interface. For the current geometry (Fig. 1*A*), this requirement favors a smaller device depth $h \ll w$ or an elongated nanowell $L \gg w$. However, reducing the device depth h requires higher pressure during the liquid loading step, which acts to reduce the operational pressure range, whereas increasing the nanowell length L leads to incomplete nanowell filling during the first stage (Fig. 1 *b2*).

Using these guidelines, a device was fabricated with nanowell dimensions of 200 μm × 400 μm × 100 μm. The droplets' volume was set to 8 nL each to provide cell concentrations of 1.25×10^5 cells per mL when a single cell is encapsulated in a droplet. To reach optimal performance, restriction thickness was minimized to be as small as possible. For this, silicone-on-insulator masters were fabricated using deep reactive ion etching (DRIE) to obtain a restriction width of 6 ± 2μm. PDMS devices were made from these molds, then their performances were characterized when sealed against either hydrophobic (polystyrene cell culture dishes) or hydrophilic (glass) substrates and tested with liquids of varying surface tensions: 0.1% Tween 20 (55 ± 3 mN/m), normal human dermal fibroblast (NHDF) cell medium (60 ± 4 mN/m), and water (72 ± 2 mN/m). For each liquid–substrate combination, the inlet loading pressure range, shearing pressure range, and average liquid flow rate were measured (Fig. 1*C*). Under various substrate/liquid surface tension combinations, a broad range of pressure levels permitting failure-free device operation has been observed. This allows for the operation of the SNDA in portable settings where the loading and shearing steps may be performed manually using either a latex bulb or a pipette.

Under some conditions, a significant overlap exists between loading and shearing pressures (Fig. 1*C*), which led us to test whether these two steps could be combined into a single operation. We found that this indeed is possible. Furthermore, by injecting a specific liquid volume matching the total droplet volume (~5 μL), it was possible to achieve 100% injection efficiency; namely, all the liquid injected was dispersed into droplets. For operation simplicity, the devices typically were loaded with 15 μL. Each nanowell was labeled with a unique number incorporated in the SNDA design to allow easy tracking of a specific droplet over time (Fig. 1*D* and Fig. S1).

Concentration Gradient Formations. Given the ability to generate stationary droplet arrays, we further investigated whether SNDAs may be used to generate stationary droplets, each with a different chemical composition. Such capability was demonstrated before,

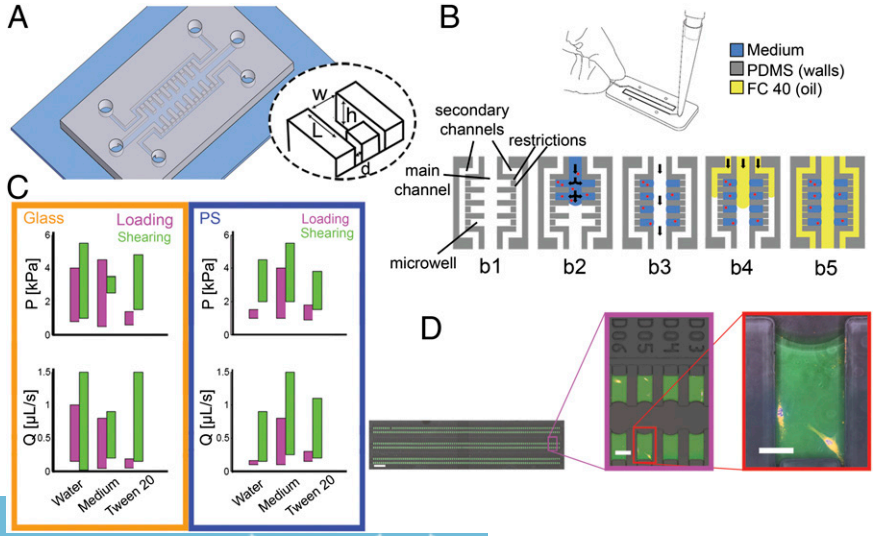

Fig. 1. Device structure, loading procedure, and characterization. (*A*) Three-dimensional device depiction. (*B*) Loading steps. (*b1*) Empty device. (*b2*) Cell-containing medium is injected into the main channel, (*b3*) air pressure shears the continuous liquid into separate droplets, and (*b4* and *b5*) fluorocarbon oil is introduced at the main and secondary inlets and flows to sheath the stationary droplets. (*C*) Device characterization under various liquid/substrate combinations. Loading pressure is the pressure applied at the inlet to drive the liquid into the nanowells during step *b2*. Shearing pressure is the pressure applied at the inlet to shear the liquid into separate stabilized droplets (*b3*). The liquids used and their corresponding surface tensions are water (72 mN/m), NHDF medium (60 mN/m), and Tween 20 0.01% (55 mN/m). Substrates used are glass and polystyrene tissue culture plate. (*D*) FITC-dextran containing medium seeded with fibroblasts visualized at three different magnifications. Hoechst 33342 and DiI were used to stain the cell membrane and nucleus. Each magnification was constructed by two separate images. [Scale bars (left to right): 2 mm, 200 μm, and 100 μm.]

Downloaded at Palestinian Territory, occupied on December 14, 2021
www.manaraa.com

with other methods (40, 41) using up to 96 stationary droplets (42). Droplets with different chemical composition have the potential to assist in miniaturized high-throughput screening assays, such as testing the influence of a growth factor concentration on cells or antibiotic concentration on bacteria. We found that producing a chemical gradient along 600 droplets is possible by using the same device prototype (8-nL droplets) while modifying the loading procedure (Fig. 2). Starting with an empty device, the modified loading procedure begins with an injection of a concentrated solute into the inlet while simultaneously injecting a low-solute concentration in the outlet where the two meet (Fig. 2*B*). The symmetry then is broken by induced unidirectional flow created by aspirating residual liquid from the outlet only, which generates a constant pressure that drives convective flow along the main channel toward the outlet. The pressure is generated without external means but rather by the nonaspirated liquid residing at the inlet, which is proportional to the column height of this liquid at the inlet. A loss of volume does not result in a significant loss of liquid height, because the inlet diameter is much larger than the channel diameter. The typical PDMS slab thickness we used was 4 mm, which corresponds to an inlet pressure of ~40 Pa. After flow was allowed to induce diffusion, the gradient was captured by shearing the main channel liquid to generate separate droplets. The gradient steepness was controlled by varying the passive convection time during the flow convection step (Fig. 2*C* and Fig. S3). By simultaneously altering this, as well as the solute concentrations introduced at the inlet/outlet, we could control both the minimal and maximal solute concentration of each drop, as well as the gradient steepness (Fig. 2 *C* and *D* and Fig. S3).

Cell Viability and Recovery. After initial characterization of the device, we set to test its ability to support single-cell incubation as well as the ability to perform common tissue culture assays on droplet-encapsulated cells. We first investigated the capacity of the SNDA platform to support live mammalian adherent cell survival for up to a few days. For this, human fibroblasts were loaded into the device at a concentration of 0.25×10^6 cells per mL, corresponding to an average of two cells per droplet. After initial injection and droplet shearing, the number of cells in each droplet was counted manually. Subsequently, cell viability and proliferation were measured over days. The viability assay was performed by removing oil from the main channel and injecting trypan blue, which selectively colors dead cells (Fig. 3*A*). We observed high viability (~90%) at all measured time points as well as proliferation by counting live and dead cells within the droplets (Fig. 3*B*).

Unlike conventional methods, which irreversibly seal a microfluidic device by treatment of oxygen plasma (20, 43, 44), in the presented method, the PDMS is attached to the substrate without permanent sealing, allowing it to be peeled from the substrate. Cells, which are adhered to the substrate, may be left to grow with the addition of culture medium. In addition, after peeling, the area of the substrate that was in contact with the PDMS becomes more hydrophobic, allowing visualization of the preexisting pattern of the wells by using hydrophobic dyes.

The ability to retrieve cells further raises the question of whether it is possible to grow the retrieved cells to interface them later with conventional cell culture techniques. Following device peeling, medium was added to the tissue culture plate and the cells were allowed to proliferate on the substrate. We observed stable proliferation capacity, and the cells retained their ability to proliferate (Fig. S4). In addition, it was possible to access the retrieved cells directly for fixation and staining. Cells were stained for nuclear Ki-67, marking cells that entered the S-phase, indicative of normal cell-cycle progression. In addition, a triple staining of DAPI, phalloidin, and vinculin showed normal cell spreading with visible focal contacts and actin filament bundles, even after cell recovery (Fig. 3 *C*–*E*).

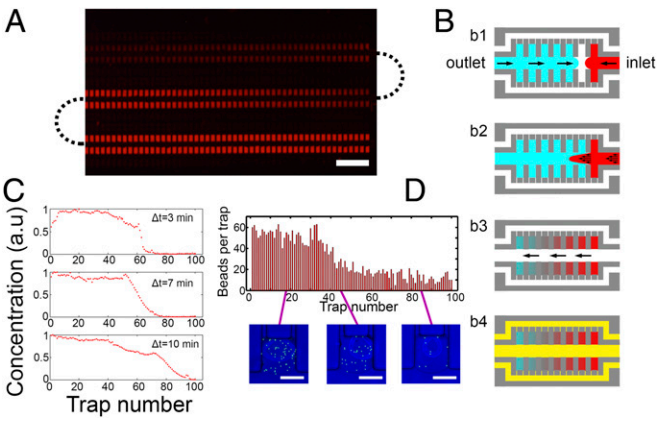

Fig. 2. Solute gradient formed in stationary droplet array. (*A*) Fluorescent bead (diameter, 100 nm) gradient. The image captures roughly half the device area. (Scale bar, 2 mm.) (*B*) Loading procedure to generate droplet gradient. Initially, two liquids with different solute concentrations are injected, one from the inlet and the other from the outlet (*b1*). Fluid convection is formed by aspirating residual liquid from the outlet but leaving a reservoir liquid plug (perpendicular to the plane of the device) at the inlet, thus forming an accurate pressure-driven flow. After the liquid is sheared, the gradient is maintained in the droplet array (*b3*) followed by oil sheathing (*b4*). (*C*) Various normalized gradient formations in 0.3-nL droplets with different steepnesses, depending on the waiting time during step *b2*. (*D*) Formation of a fluorescent bead (diameter, 1 μm) gradient in 0.3-nL droplets. Images show various bead concentrations taken from three representative positions along the device. (Scale bars, 50 μm.)

Bacterial and Mouse Leukemia Cell Proliferation. To investigate the capacity of SNDAs to support proliferation of encapsulated cells, we loaded droplets with nonadherent mammalian and bacterial cells in 8-nL and 0.3-nL droplets, respectively, and monitored cell proliferation over time. Nonadherent mouse leukemia cells (L1210) were encapsulated at an initial concentration of zero to four cells per droplet; in each nanowell, the number of cells was counted every 12 h over 48 h. Proliferation was observed, in some cases surpassing a tenfold increase over a 48-h period (Fig. 4 *A* and *B*), similar to rates observed for these cells in conventional cultures (45).

For bacterial cells, *Escherichia coli* cells were encapsulated in a different prototype that was designed with nanowell dimensions of 80 μm × 80 μm × 50 μm, corresponding to ~0.3 nL each. To simplify observation and cell counting, the *E. coli* cells were transformed with a GFP (pGreenTIR)-expressing plasmid (46). *E. coli* proliferation was tracked in a total of 100 droplets over 8 h by using time-lapse microscopy (Fig. 4 *C* and *D* and Movie S2). It was found that droplets containing a similar initial cell number could still follow diverse replication patterns during the 8 h, leading to a large variation in the end-point cell number. Because all the microenvironmental conditions were similar, this variation might be attributed to cell heterogeneity manifested by a variation in the endogenous replication rate of the individual bacterium.

Single-Fibroblast Metabolic Assay Discretization. The droplets' chemical isolation was used to implement a single-cell performance-based assay. For this, we chose to investigate the metabolic activity of fibroblasts (NHDF) using the alamarBlue assay, which is used routinely to estimate the number of metabolically active cells in bulk (47). In the presence of a live cell, its fluorescence turnover linearly increases over time. The linearity coefficient corresponds to the number of live cells. Cell number per droplet obeys a Poisson distribution because of the statistical nature of the encapsulated cells (Fig. S5). Cell concentration was set to an average

Downloaded at Palestinian Territory, occupied on December 14, 2021
www.manaraa.com

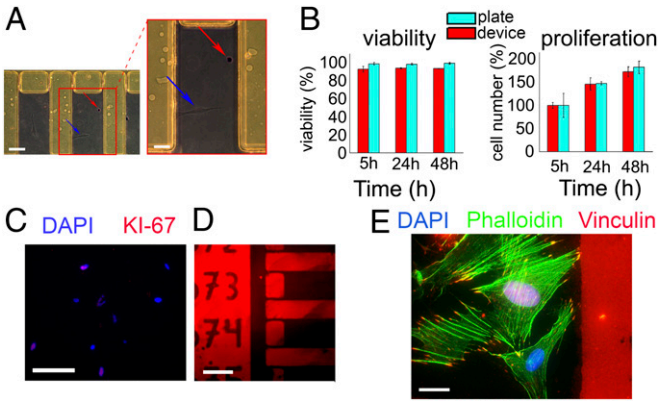

Fig. 3. Adherent cell (fibroblast) viability, proliferation, and recovery. (*A*) On-chip viability assay (trypan blue) at a single droplet. The zoomed picture shows a round dead trypan blue-stained cell (red arrow) and an unstained live fibroblast (blue arrow). (Scale bars, 100 μm and 50 μm.) (*B*) In-droplet cell viability and proliferation sampled at three time points (t = 5 h, 24 h, 48 h) and over 200 droplets (device). Cell-seeded plates using the same initial cell concentration were used as controls. (*C*) Ki-67 nuclear staining of recovered adherent cells 8 d after device peeling. (Scale bar, 100 μm.) (*D*) Nonspecific staining of substrate by antivinculin in hydrophobic areas following PDMS removal, revealing the intact device pattern, thus allowing retrieval of a cell of choice. (*E*) Off-chip triple staining of recovered fibroblasts (DAPI, phalloidin, vinculin) initially grown in 8-nL droplets for 24 h. Appearing on the right is nonspecific phalloidin staining of the area in which the PDMS was in contact with the substrate. (Scale bar, 20 μm.)

of two cells per droplet to achieve a large sample size of droplets containing zero, one, two, and three cells per droplet. Fluorescence was monitored in the initial linear regime for up to 5 h at a sampling rate of 5 min (Fig. 5 *A* and *B*). Only droplets in which the cell number did not change during this period were used for analysis. We quantified the fluorescence increase over six experiments of 200 nanowells each. For a given droplet, the number of cells encapsulated was proportional to the corresponding fluorescent buildup (Fig. 5*C*). The results show a significant difference ($P < 0.05$) for nanowells containing zero, one, two, or three cells per droplet, indicating that cell metabolic activity may be detected at the single-cell level by using this device (Fig. 5*C*, Table S1, and Movies S3 and S4). SNDAs therefore may be used for performance-based assays involving fluorescent cell metabolite secretion, which requires long cell incubation. It also allows characterization of single-cell contributions to the entire cell population response.

Using this same assay while monitoring cell morphology in parallel further revealed that a single cell's spread area was correlated with its fluorescence buildup, with larger cells having higher metabolic activity (Fig. 5*D*). Moreover, we found a correlation between cell branching (circumference^2/area) and the redox potential of the cells. Interestingly, cells with higher branching (higher than the median) revealed a significant increase (35%, $P = 0.0028$) in fluorescence buildup rate compared with more rounded cells (lower than the median).

Digital Concentration Detection of *Staphylococcus aureus* Colony-Forming Units. *S. aureus* bacteremia is an important infection as it has a mortality rate higher than that of AIDS, tuberculosis, and viral hepatitis combined (48). Given its clinical relevance, we explored whether live pathogen concentration in a sample can be determined. First, the viability of *S. aureus* was verified in the device, as well as its capacity to support colony formation in droplets originating from a single cell (Fig. 6 *A* and *B*). We then checked whether it is possible to deduce the viable pathogen concentration in a sample based on the number of colony-formed droplets. For this evaluation, a blood sample was spiked with *S. aureus* at various cell concentrations, all with averages much lower than one cell per droplet. We injected the sample into the device and counted the number of colonized droplets after culture at 37 °C for 20 h. We found that the number of colonies formed was correlated with the pathogen number initially injected into the devices (Fig. 6*D*) and that we could detect pathogen concentration as low as 560 cfu/mL. This detection limit may be lowered by an order of magnitude or more by increasing the total number of droplets or their volume or by injection to multiple devices at once. Because of the SNDA's low reagent consumption, the total number of *S. aureus* cells used to perform all the experiments summarized in Fig. 6*D*, including duplicates, was less than 2,000.

Discussion

For single-cell analysis, SNDAs offer several advantages over conventional methods. They easily generate hundreds of stationary, indexed, nanoliter droplets, providing a simple way to set up and perform cell-encapsulated assays that require long-scale single-cell tracking over time. These advantages make SNDAs a practical research or diagnostic tool for applications that depend on measuring long-timescale cellular processes. The SNDA uses a unique loading procedure operated in reverse order, in which the dispersed medium is injected first and sheared into droplets, and only later is a continuous phase injected for droplet sheathing. This reverse-loading process creates two distinct interfacial energy values: one for the liquid–gas interface and the other for the liquid–solid interface. By adjusting the nanowell geometry, this interfacial energy difference may be used to both shear continuous liquid into separate droplets and optimize droplet trapping.

The end result is a stationary droplet array composed of hundreds of droplets in nanowells, in which each nanowell has a unique index. These stationary droplets can support adherent cells by being in contact with a cell culture substrate. This inexpensive and portable technology, which does not require the complex instrumentation and sensitive pressure control of traditional droplet microfluidics, makes single-cell experiments accessible to every laboratory.

Two prototypes were designed: one with 600 8-nL droplets and a second, smaller prototype with 200 0.3-nL droplets. We

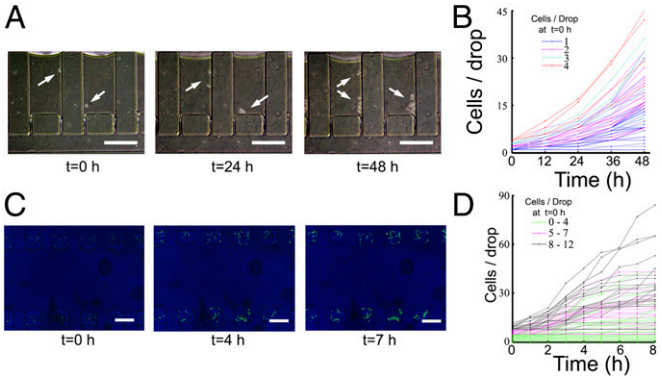

Fig. 4. In-droplet single-cell proliferation. (*A*) Mouse leukemia cell proliferation in 8-nL droplets imaged at t = 0 h, 24 h, and 48 h. Arrows indicate cell positions. (Scale bars, 200 μm.) (*B*) Mouse leukemia growth curves in single droplets up to 48 h. Sampling rate is 12 h. Curves are color indexed based on the cell number per droplet at t = 0 h. (*C*) *E. coli* proliferation in eight 0.3-nL droplets observed under 20× magnification over the course of 7 h. (Scale bars, 100 μm.) (*D*) *E. coli* growth curve in single droplets tracked under a 40× objective over 8 h. Sampling rate is 1 h. Single curves are color indexed based on the number of cells per droplet at t = 0 h. For cell/droplet values >30 and >50, cell counting error due to bacteria aggregation is estimated to be ±4 and ±10, correspondingly.

Downloaded at Palestinian Territory, occupied on December 14, 2021
www.manaraa.com

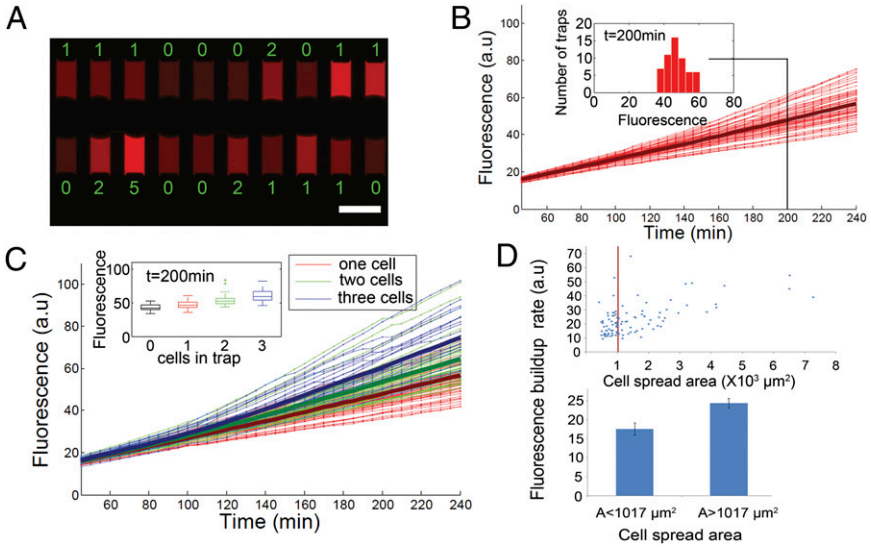

Fig. 5. Single-cell alamarBlue metabolic assay. (*A*) Single image of 20 cell-encapsulating droplets with alamarBlue. Image was taken at $t = 240$ min. The cell number per droplet appears near each nanowell. (Scale bar, 400 μm.) (*B*) Fluorescence quantification of droplets containing a single cell. Each line represents a droplet. The average appears in bold. (*Inset*) Fluorescence distribution at $t = 200$ min. (*C*) Quantification of fluorescence buildup over time for droplets containing one, two, and three cells per droplet. Average values for each group appear in bold. (*Inset*) Boxplot of the fluorescence at $t = 200$ min. (*D*) Correlation between cell spread area and alamarBlue fluorescence buildup. The cutoff between the two groups in the bar graph was the median, corresponding to a cell spread area of 1,017 μm ($P = 0.0002$).

characterized the device performance and found it to have a low dependence on the substrate and type of liquid used. We showed that a stationary droplet solute concentration gradient can be generated while controlling interdroplet chemical gradient steepness. Such a gradient has high relevancy in screening assays and may be used to rapidly characterize the time response of single rare cells. We demonstrated both mammalian adherent (fibroblasts) and nonadherent (mouse leukemia) as well as prokaryotic (*E. coli*, *S. aureus*) single cell-incubation and proliferation during hours up to days. Recovered adherent cells also can be grown off-chip and therefore interfaced with common tissue-culture techniques.

We used the droplets' chemical isolation to assess single-cell metabolic activity with the fluorogenic alamarBlue assay. We observed different fluorescence buildup rates due to the presence of one, two, or three cells per droplet. This demonstrates that unlike conventional bulk assays, in which the performance of the cell population is measured in bulk and analyzed through a single channel, the SNDA allows multichannel readout in which continuous quantification of an adherent cell population on the single-cell level is possible. Specifically in this work, hundreds of channels were investigated, each representing the behavior of a single adherent cell's metabolic activity. In this assay, we use the ability of the SNDA to create isolated microenvironments for single adherent cells directly on tissue culture substrates to track the redox potential, through the buildup of alamarBlue fluorescence within the wells, during the cell adhesion process. In our experiment, we started tracking the fluorescence buildup of alamarBlue at a critical time when the cells have not yet adhered or are in the early stages of doing so. We then continued to track the buildup throughout the adhesion process. The unchanging slopes of the plots in Fig. 5*B* during cell adhesion confirm the steady nature of the redox potential, an important parameter that gives insight into cellular health and metabolism. Interestingly, when we coupled this assay to image analysis data of cell shape, we found that the metabolic activity is related to the cell's spread area and shape, with higher fluorescent buildup in the larger cells and in cells with higher branching.

The ability to capture a single live *S. aureus* in droplets and expand it to a colony that fills the droplet after 48 h also was demonstrated here. We showed that it is possible to quantify the initial live pathogen sample concentration based on the number of colonies formed down to a detection limit of 560 cfu/mL while using very low total cell number.

The method presented offers a simple yet robust device for generating nanodroplet arrays by using a few microliters of reagent and hundreds of cells. The pressure insensitivity of the SNDA makes it compatible with manual operation in portable

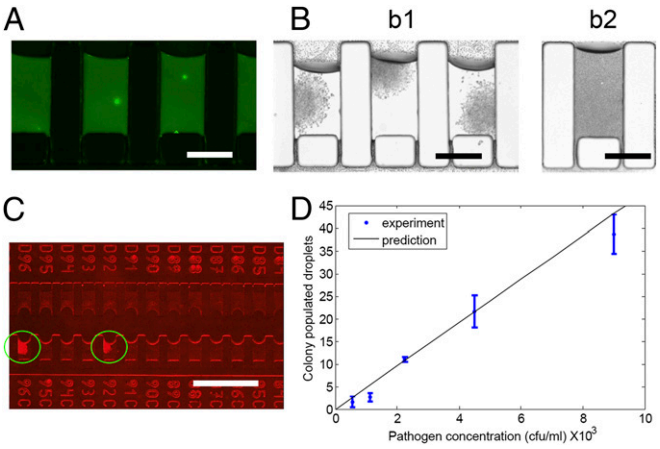

Fig. 6. *S. aureus* colony formation in droplets. (*A*) A single pathogen (green) encapsulated in 8-nL droplets. Viability was verified with a live/dead assay. (Scale bar, 200 μm.) (*B*) Colonies formed from each single cell trapped in wells of the device after culture for 24 h (*b1*) and for 48 h (*b2*). (Scale bars, 200 μm.) (*C*) Colony formation in whole blood spiked with live *S. aureus* at a pathogen concentration of 4.5 × 103 cfu/mL. Green circles indicate droplets in which colonies were formed. (Scale bar, 1 mm.) (*D*) Correlation between the initial pathogen concentration in blood and the number of colony-populated droplets measured after 20-h incubation. Error bars indicate SE mean, $n = 3$.

Downloaded at Palestinian Territory, occupied on December 14, 2021
www.manaraa.com

or resource-poor settings where sophisticated pressure-regulating equipment is unavailable. The method does not require the use of potentially cytotoxic surfactants, allows easy adherent cell retrieval of choice, and may be used with different substrates, such as glass and tissue culture plate (polystyrene). This method also may be used to generate a high-resolution stationary droplet chemical gradient.

The ability to rapidly and easily set up SNDAs, especially suitable for adherent cell culture, may help bring new single-cell assays to biological laboratories unfamiliar with or unequipped for microfluidic work. This capability may further contribute to research involving cellular characterization, such as immunological cell-to-cell communication, and analysis of heterogeneous cell responses.

Materials and Methods

For detailed materials and methods, see *SI Materials and Methods*. Device loading was operated by using a bulb/pipette or vacuum applied at the outlet. In all experiments, a biocompatible fluorocarbon oil (Fluorinert FC40, F9755-100ML; Sigma) was used without any added fluorosurfactant. Before loading, each device was washed, air blown, cleaned with adhesive tape, and sealed against a TC plate or coverslip. To reduce evaporation, devices were primed with double distilled water at 60 °C for 0.5 h and centrifuged at $500 \times g$ for 1 min to remove adhered bubbles. Water priming was repeated, and devices were stored at 37 °C overnight. To reduce evaporation during an experiment, the main channel's inlet and outlet were sealed with adhesive tape, and water was added to the plate to cover the device's sides and upper surface.

ACKNOWLEDGMENTS. We thank Galia Ben-David for technical assistance and the laboratory members for help with biological assays and valuable discussions. We thank Avshalom Shai from the Technion Micro Nano Fabrication Unit for DRIE process design and fabrication and Nitsan Dahan from the Life Sciences and Engineering Infrastructure Center, Microscopy Unit, Technion for his technical assistance. We thank Adi Guterman for technical support in *E. coli* experiments, Sima Yaron for providing PVS PG 1T1R EGFP plasmid, and Itamar Simon and Oded Sandler for providing leukemia mouse cells. We thank Alexander Diaz (Wyss Institute) for technical assistance. This work was funded by the Israel Ministry of Science Tashtiot grant and by the Russell Berrie Nanotechnology Institute Seed Funds–Nevet Program, Technion.

1. Bendall SC, et al. (2011) Single-cell mass cytometry of differential immune and drug responses across a human hematopoietic continuum. *Science* 332(6030):687–696.
2. Ma C, et al. (2011) A clinical microchip for evaluation of single immune cells reveals high functional heterogeneity in phenotypically similar T cells. *Nat Med* 17(6): 738–743.
3. Varadarajan N, et al. (2012) Rapid, efficient functional characterization and recovery of HIV-specific human CD8+ T cells using microengraving. *Proc Natl Acad Sci USA* 109(10):3885–3890.
4. Rane TD, Zec HC, Puleo C, Lee AP, Wang TH (2012) Droplet microfluidics for amplification-free genetic detection of single cells. *Lab Chip* 12(18):3341–3347.
5. Um E, Rha E, Choi SL, Lee SG, Park JK (2012) Mesh-integrated microdroplet array for simultaneous merging and storage of single-cell droplets. *Lab Chip* 12(9):1594–1597.
6. Schmitz CH, Rowat AC, Köster S, Weitz DA (2009) Dropspots: A picoliter array in a microfluidic device. *Lab Chip* 9(1):44–49.
7. Moon S, et al. (2011) Drop-on-demand single cell isolation and total RNA analysis. *PLoS One* 6(3):e17455.
8. Brouzes E, et al. (2009) Droplet microfluidic technology for single-cell high-throughput screening. *Proc Natl Acad Sci USA* 106(34):14195–14200.
9. Fan HC, Wang J, Potanina A, Quake SR (2011) Whole-genome molecular haplotyping of single cells. *Nat Biotechnol* 29(1):51–57.
10. Warren L, Bryder D, Weissman IL, Quake SR (2006) Transcription factor profiling in individual hematopoietic progenitors by digital RT-PCR. *Proc Natl Acad Sci USA* 103(47):17807–17812.
11. Heyries KA, et al. (2011) Megapixel digital PCR. *Nat Methods* 8(8):649–651.
12. Bransky A, Korin N, Khoury M, Levenberg S (2009) A microfluidic droplet generator based on a piezoelectric actuator. *Lab Chip* 9(4):516–520.
13. Baret JC, et al. (2009) Fluorescence-activated droplet sorting (FADS): Efficient microfluidic cell sorting based on enzymatic activity. *Lab Chip* 9(13):1850–1858.
14. Churski K, Korczyk P, Garstecki P (2010) High-throughput automated droplet microfluidic system for screening of reaction conditions. *Lab Chip* 10(7):816–818.
15. Niu X, Gielen F, Edel JB, deMello AJ (2011) A microdroplet dilutor for high-throughput screening. *Nat Chem* 3(6):437–442.
16. Shemesh J, Nir A, Bransky A, Levenberg S (2011) Coalescence-assisted generation of single nanoliter droplets with predefined composition. *Lab Chip* 11(19):3225–3230.
17. El Debs B, Utharala R, Balyasnikova IV, Griffiths AD, Merten CA (2012) Functional single-cell hybridoma screening using droplet-based microfluidics. *Proc Natl Acad Sci USA* 109(29):11570–11575.
18. Huebner A, et al. (2009) Static microdroplet arrays: a microfluidic device for droplet trapping, incubation and release for enzymatic and cell-based assays. *Lab Chip* 9(5): 692–698.
19. Abbyad P, Dangla R, Alexandrou A, Baroud CN (2011) Rails and anchors: Guiding and trapping droplet microreactors in two dimensions. *Lab Chip* 11(5):813–821.
20. Theberge AB, et al. (2010) Microdroplets in microfluidics: an evolving platform for discoveries in chemistry and biology. *Angew Chem Int Ed Engl* 49(34):5846–5868.
21. Zhan Y, Wang J, Bao N, Lu C (2009) Electroporation of cells in microfluidic droplets. *Anal Chem* 81(5):2027–2031.
22. Wang W, Yang C, Liu Y, Li CM (2010) On-demand droplet release for droplet-based microfluidic system. *Lab Chip* 10(5):559–562.
23. Cohen DE, Schneider T, Wang M, Chiu DT (2010) Self-digitization of sample volumes. *Anal Chem* 82(13):5707–5717.
24. Han Q, Bradshaw EM, Nilsson B, Hafler DA, Love JC (2010) Multidimensional analysis of the frequencies and rates of cytokine secretion from single cells by quantitative microengraving. *Lab Chip* 10(11):1391–1400.
25. Boukellal H, Selimović S, Jia Y, Cristobal G, Fraden S (2009) Simple, robust storage of drops and fluids in a microfluidic device. *Lab Chip* 9(2):331–338.
26. Lecault V, et al. (2011) High-throughput analysis of single hematopoietic stem cell proliferation in microfluidic cell culture arrays. *Nat Methods* 8(7):581–586.
27. Taylor RJ, et al. (2009) Dynamic analysis of MAPK signaling using a high-throughput microfluidic single-cell imaging platform. *Proc Natl Acad Sci USA* 106(10):3758–3763.
28. Bai Y, et al. (2013) Intra-species bacterial quorum sensing studied at single cell level in a double droplet trapping system. *Int J Mol Sci* 14(5):10570–10581.
29. Dewan A, Kim J, McLean RH, Vanapalli SA, Karim MN (2012) Growth kinetics of microalgae in microfluidic static droplet arrays. *Biotechnol Bioeng* 109(12):2987–2996.
30. Iino R, Matsumoto Y, Nishino K, Yamaguchi A, Noji H (2013) Design of a large-scale femtoliter droplet array for single-cell analysis of drug-tolerant and drug-resistant bacteria. *Front Microbiol* 4:300.
31. Konry T, Golberg A, Yarmush M (2013) Live single cell functional phenotyping in droplet nano-liter reactors. *Sci Rep* 3:3179.
32. Leung K, et al. (2012) A programmable droplet-based microfluidic device applied to multiparameter analysis of single microbes and microbial communities. *Proc Natl Acad Sci USA* 109(20):7665–7670.
33. Nguyen CQ, Ogunniyi AO, Karabiyik A, Love JC (2013) Single-cell analysis reveals isotype-specific autoreactive B cell repertoires in Sjögren's syndrome. *PLoS One* 8(3): e58127.
34. Ricicova M, et al. (2013) Dissecting genealogy and cell cycle as sources of cell-to-cell variability in MAPK signaling using high-throughput lineage tracking. *Proc Natl Acad Sci USA* 110(28):11403–11408.
35. Sendra VG, Lie A, Romain G, Agarwal SK, Varadarajan N (2013) Detection and isolation of auto-reactive human antibodies from primary B cells. *Methods* 64(2):153–159.
36. Avesar J, Arye TB, Levenberg S (2014) Frontier microfluidic techniques for short and long-term single cell analysis. *Lab Chip* 14(13):2161–2167.
37. Gabriel JL, Miller TF, Jr, Wolfson MR, Shaffer TH (1996) Quantitative structure-activity relationships of perfluorinated hetero-hydrocarbons as potential respiratory media. Application to oxygen solubility, partition coefficient, viscosity, vapor pressure, and density. *ASAIO J* 42(6):968–973.
38. Holtze C, et al. (2008) Biocompatible surfactants for water-in-fluorocarbon emulsions. *Lab Chip* 8(10):1632–1639.
39. Berthier J (2008) *Microdrops and Digital Microfluidics* (William Andrew, Norwich, NY).
40. Laval P, Lisai N, Salmon JB, Joanicot M (2007) A microfluidic device based on droplet storage for screening solubility diagrams. *Lab Chip* 7(7):829–834.
41. Sun M, Bithi SS, Vanapalli SA (2011) Microfluidic static droplet arrays with tuneable gradients in material composition. *Lab Chip* 11(23):3949–3952.
42. Fradet E, et al. (2011) Combining rails and anchors with laser forcing for selective manipulation within 2D droplet arrays. *Lab Chip* 11(24):4228–4234.
43. Song H, Chen DL, Ismagilov RF (2006) Reactions in droplets in microfluidic channels. *Angew Chem Int Ed Engl* 45(44):7336–7356.
44. Huebner A, et al. (2008) Microdroplets: A sea of applications? *Lab Chip* 8(8): 1244–1254.
45. Tovey MG, Rochette-Egly C, Castagna M (1980) Correlation between growth rate, cell density, and intracellular concentrations of cyclic nucleotides in chemostat cultures of mouse L1210 cells. *J Cell Physiol* 105(2):363–367.
46. Miller WG, Lindow SE (1997) An improved GFP cloning cassette designed for prokaryotic transcriptional fusions. *Gene* 191(2):149–153.
47. Voytik-Harbin SL, Brightman AO, Waisner B, Lamar CH, Badylak SF (1998) Application and evaluation of the alamarBlue assay for cell growth and survival of fibroblasts 34(3):239–46.
48. van Hal SJ, et al. (2012) Predictors of mortality in Staphylococcus aureus bacteremia. *Clin Microbiol Rev* 25(2):362–386.

Downloaded at Palestinian Territory, occupied on December 14, 2021
www.manaraa.com